CrystEngComm

Accepted Manuscript

ROYAL SOCIETY OF CHEMISTRY

www.rsc.org/crystengcomm

CrystEngComm RSCPublishing

ARTICLE

One-Step Synthesis of High-Quality Homogenous Te/Se Alloy Nanorods with Various Morphologies

Cite this: DOI: 10.1039/x0xx00000x

Shilin Fu,[a] Kai Cai[a], Long Wu[a] and Heyou Han[a,*]

Received 00th January 2012,
Accepted 00th January 2012

DOI: 10.1039/x0xx00000x

www.rsc.org/

A convenient method was developed for controllable synthesis of homogeneous trigonal Te/Se alloy nanorods (t-Te/Se ANRs) with diverse morphologies, aspect ratios and compositions at room temperature within aqueous solution. These alloy nanorods were formed by a self-seeding process. By varying the molar ratio of TeO2 to H2SeO3 (x(Te:Se)) in the initial precursors, the morphology of t-Te/Se ANRs was transformed mainly in two paths: the formation of tri-fold nanorods (TNRs) or single nano-rods (SNRs). The nanostructures of TNRs generated only with x(Te:Se) ranging from 30:1 to 10:1, and SNRs formed with x(Te:Se) ranging from 200:1 to 100:1 or 2:1 to 1:1. The microstructures, compositions, and growth mechanisms of these nanorods were also analyzed in detail.

Introduction

Tellurium (Te) and Selenium (Se) are p-type semiconductors with a narrow band gap and high activity in hydration and oxidation reactions, in which Te, Se and Te/Se alloy are utilized in the fields of gas sensor, thermoelectricity, photoconductivity and template method synthesis.[1-10] Te/Se alloy is composed of composite Te-Se atom-bonded helical chains, which are randomly united via van der Waals force as highly anisotropic crystal structures.[11-13] Particularly, nanodevices based on Te/Se alloy have many stimulating properties superior to pure Te and Se nanomaterials in electrical resistance and magnetoresistance.[10, 11, 14, 15] The morphologies of Te and Se nanostructures, just like Te or Se nanorods, have been extensively investigated in previous studies.[2, 13, 16-30] However, the study of t-Te/Se ANRs is still in its primitive stage in terms of morphology diversity, uniformity and synthesis method.[31-35] Currently, little information is available about the morphology of trigonal Te/Se alloy tri-fold nanorods (t-Te/Se ATNRs). For the sake of expanding the category of Te/Se alloy nanocrystals, recent research has been devoted to controllable synthesis of this homogeneous semiconductor nanocrystal.

Both trigonal tellurium (t-Te) and trigonal selenium (t-Se) belong to the hexagonal-trigonal crystal system, and are very identical to each other in crystal form.[11, 13] Pure tellurium dioxide and selenious acid can be easily crystallized together into hexagonal nanoplatelets because of the anisotropic and isomorphous characteristics of Te and Se.[11] The produced Te and Se atoms tend strongly to grow randomly along the c-axis of crystal lattice to form nanorods through a homogeneous nucleation and self-seeding process.[11, 13] Te and Se, albeit with similar chemical, physical and crystalline properties, also have some differences in those aspects as well, resulting in the growth of t-Te/Se ANRs different from either Te or Se nanostructures, such as the synthesis of t-Te/Se ATNRs in a certain molar proportion range of Te and Se precursors.[31]

Herein, we demonstrate a facile one-pot solution approach to synthesis various morphologies t-Te/Se ANRs with well-defined shapes, uniform sizes and large quantities. The growth mechanisms and microstructures of the morphologies of t-Te/Se ANRs were also investigated in detail. This research provides a convenient route to controllable synthesis of homogeneous t-Te/Se ANRs with diverse morphologies, aspect ratios, compositions and lattice constants, which may promise the potential application in photoconductive and thermoelectric fields.[2, 28]

EXPERIMENTAL SECTION

Materials

Tellurium dioxide (TeO_2, Aladdin, 99.99%), selenious acid (H_2SeO_3, Alddin, 99.99%), sodium dodecyl sulfate (SDS, Aldrich, 99.99%) and hydrazine monohydrate ($N_2H_4H_2O$, Sinopharm, 85%, AR) were used as purchased. The 18 MΩ cm deionized water (E-Pure, Dubuque, IA) was used during the whole experiment process.

Synthesis of t-Te/Se ANRs

TeO_2 powder and H_2SeO_3 (aqueous solution 0.2 M) were placed in a glassware and mixed fully before the reaction began. The integral molar ratio of TeO_2 and H_2SeO_3 was 0.1 mmol, which was supplemented with 10 mL of $N_2H_4H_2O$ in the reaction container by constant stirring and kept in a water bath at 33℃ for 30 min. The reaction was terminated by adding the as-prepared products into 50 mL the SDS solution (10 mM) to stabilize the products, followed by washing the unreacted mixtures and SDS by centrifugation.

Characterization methods

High-resolution transmission electron microscope (HRTEM) images and Energy-dispersive X-ray spectroscopy (EDS) spectra were obtained with a JEOL JEM 2100F electron microscope operated at 200 KeV. The Raman spectra were carried out via Raman spectrometer (Renishaw, UK) equipped with a confocal microscope (Leica, German) using an Ar laser

(514.5 nm).The energy dispersive X-ray fluorescence analyzer (EDAX) spectra were acquired by EAGLE III at 38 KeV for elemental analysis. Powder X-ray diffraction (XRD) data were collected on a Bruker D8 Advance diffractometer with Ni-filtered Cu K_α radiation (40 kV, 40 mA, λ =0.15418 nm). The UV-visible (UV-vis) absorption spectra of as-prepared t-Te/Se ANRs suspensions were recorded using a UV-vis spectrophotometer (PerkinElmer Lambda 25) over the spectral range of 200-900 nm.

Results and discussion

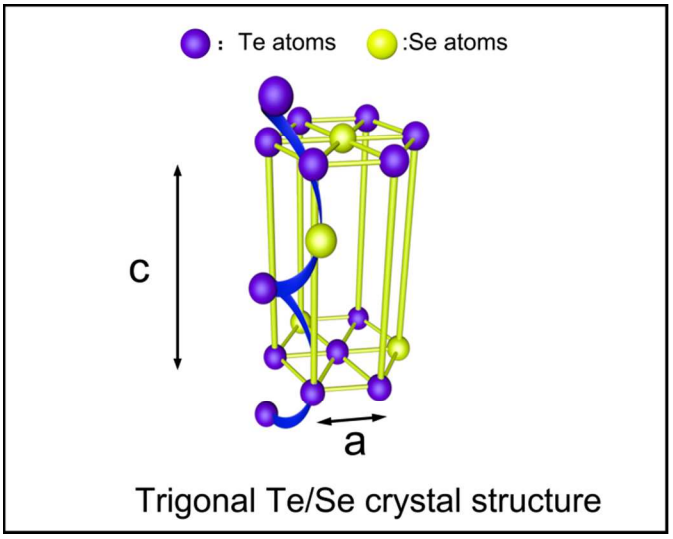

Fig. 1 The schematic of trigonal Te/Se crystal structure.

Fig. 1 shows that the Te and Se atoms can randomly form trigonal homogeneous crystals because of their identical hexagonal crystal structures; the hexagonal crystal structure consists of Te-Se bonded helical chains which benefit the highly anisotropic crystal structure of t-Te/Se ANRs.[11, 13]

The t-Te/Se ANRs were synthesized by reducing TeO_2 and H_2SeO_3 simultaneously in the presence of excess $N_2H_4H_2O$ within the aqueous medium through hydrothermal reaction:

$$xTeO_2 + yH_2SeO_3 + (x+y)N_2H_4 \rightarrow Te_xSe_y + (x+y)N_2 + (2x+3y)H_2O$$

In a typical procedure, the TeO_2 powder and aqueous solution of H_2SeO_3 were mixed fully before the $N_2H_4H_2O$ was added into the glassware to ensure the uniformity of the products. The reaction was processed in water bath under constant stirring. The colour of the reaction changed rapidly even at low temperature from colourless to brown within 30 seconds, then turned dark brown and finally nearly dark. This phenomenon was different from either pure TeO_2 which changed from colourless to purple and then to blue, or H_2SeO_3 which changed from colourless to reddish and then to brick-red opaque.[21, 26] This change indicated the t-Te/Se ANRs was produced at the initial moment, so the colour of the aqueous solution turned out to be brown rather than violet or reddish-red at the initial moment of reaction.

Morphologies of t-Te/Se ANRs

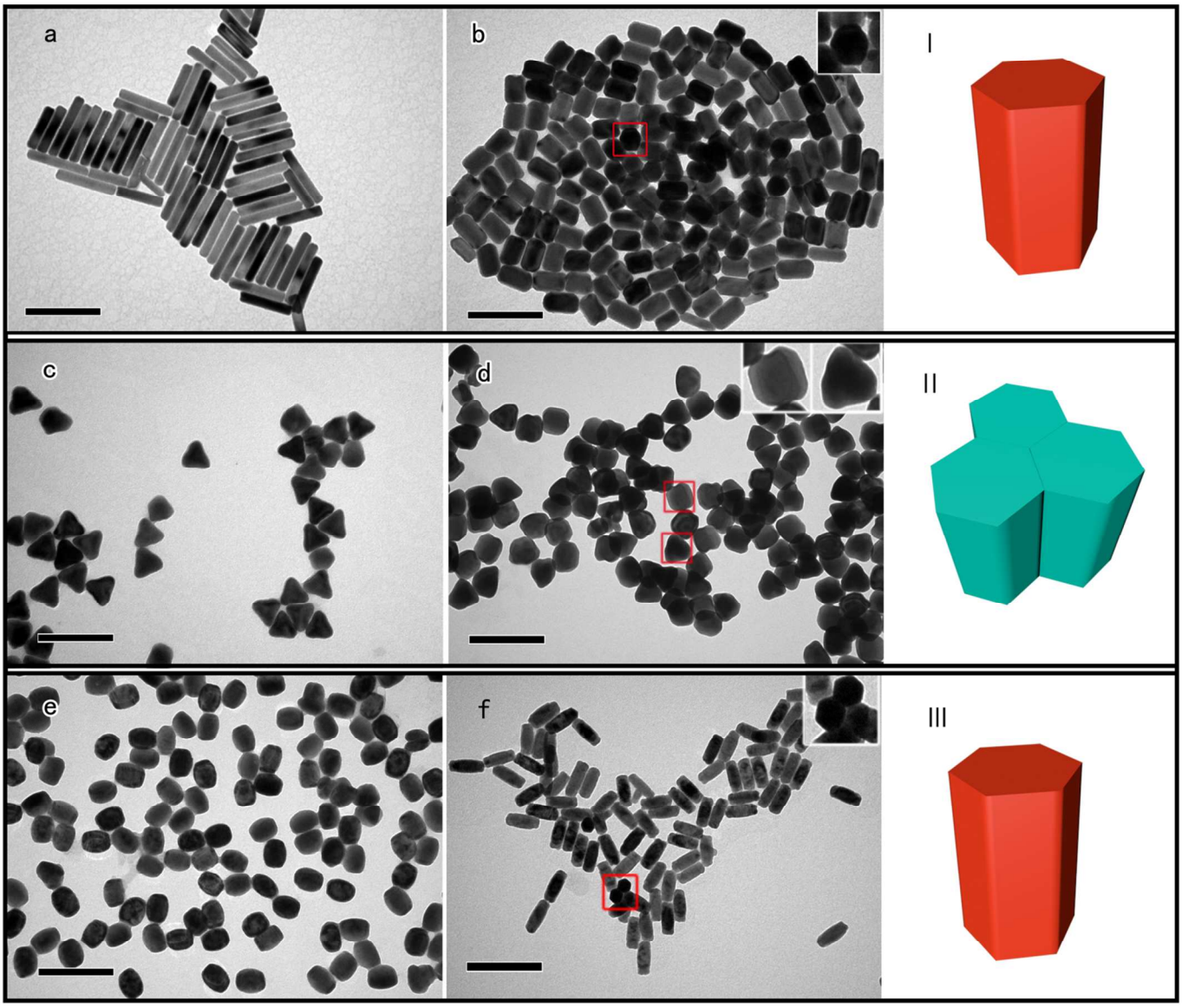

Fig. 2 TEM images of t-Te/Se ANRs generated with different values of x(Te:Se). (a) 200:1, (b) 100:1, (c) 30:1, (d) 10:1, (e) 2:1 and (f) 1:1. The insets in (b), (d) and (f) show the exact cross section morphologies of nanorods. Schema Ⅰ represents (a) and (b), Ⅱ (c) and (d), and Ⅲ (e) and (f). The scale bars in the pictures represent 200 nm.

The initial molar ratios of TeO_2 to H_2SeO_3 played a vital role in the nanostructures and aspect ratios of t-Te/Se ANRs. Fig. 2 illustrates that the TNRs only occurred with the x(Te:Se) ranging from 30:1 to 10:1 (Fig. 2c and d), and the TNRs morphology was actually combined by three small hexagonal prisms as depicted in Fig. 2 Ⅱ. However, once beyond that value, the t-Te/Se ANRs were SNRs (Fig. 2a, b, e and f). Fig. 2 Ⅰ and Ⅲ show the schematics of the SNRs. All of the t-Te/Se ANRs are distinct in shapes, monodisperse in structure and uniform in size.

When the values of x(Te:Se) were relatively high, such as 200:1 (Fig. 2a) and 100:1 (Fig. 2b), the morphologies of the t-Te/Se ANRs were SNRs. Inset in Fig. 2b shows the hexagonal cross section of the SNRs which was highlighted by the red frame. The trigonal Te/Se alloy single nanorods (t-Te/Se ASNRs) tended to have a lower aspect ratio than the pure Te nanorods, but a higher aspect ratio than the amorphous Se.[21, 26] Hence, compared to previous work, it can be concluded that the addition of a small proportion of Se to pure Te nanowires (Te NWs) reduced the length of Te NWs.

It is worth noting that when x(Te:Se)=30:1 to 10:1, the SNRs were converted into TNRs (Fig. 2c and d). And the morphologies changes little from Figure 2c to Fig. 2d. The insets in Fig. 2d show clear views of the vertical section and the cross section, with the left inset displaying the magnification of the vertical section view highlighted by the upper red frame, and the right inset illustrating the magnified TEM image of the cross-sectional view of the TNRs marked by the lower red frame. Fig. 2 Ⅱ is the 3-dimensional schematic showing the exact tri-hexagon shape of the TNRs. The t-Te/Se ATNRs could only be generated within a specific value range of x(Te:Se) which probably due to the weaker crystalline nature of Se than Te. With a higher proportion of Se, this resulted in the decrease of crystallization speed and further facilitated the separate nucleation.

To further decrease the value of x(Te:Se) to 2:1 and 1:1, the morphologies of t-Te/Se ANRs turned out to be that of SNRs again (Fig. 2e, f). Their shapes turned out to be a little shuttle-like, with the central section wider, and the aspect ratios became higher. This was probably because more Se facilitated both the amorphous and trigonal tendency of Se element in the t-Te/Se ANRs, leading to the middle expanded and the length longer of the nanocrystals.[10] However, when the x(Te:Se) dropped to 1:10 (Fig. S1, ESI†), we could only observe some spherical colloids at 10 min and nothing detectable at 30 min, also probably due to the weaker crystalline nature of Se than Te. Therefore, with a higher proportion of Se in the Te/Se alloy, the amorphous nature dominated the crystallization, leading to the formation of amorphous Te/Se (a-Te/Se) alloys with free energy higher than that of the t-Te/Se ANRs, and as the redox reaction proceeded, the a-Te/Se was converted into Te^{2+} and Se^{2+} by the reduction of excess $N_2H_4H_2O$.[21]

Characterizations

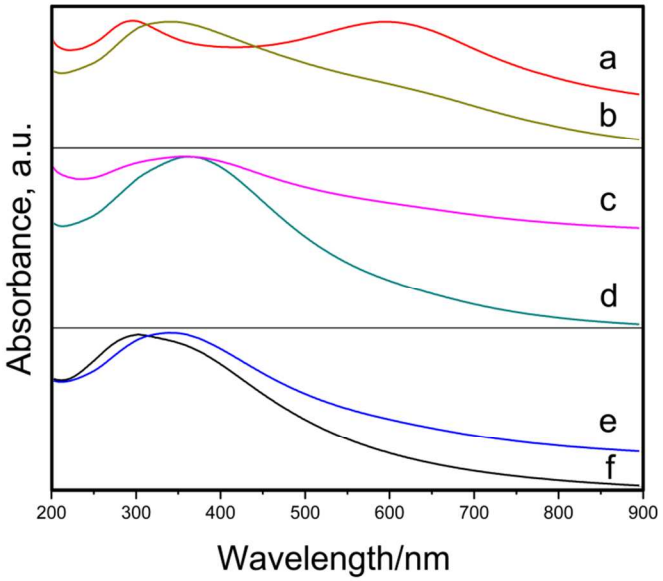

Fig. 3 UV-vis spectra of the t-Te/Se ANRs with x(Te:Se) values of (a) 200:1, (b) 100:1, (c) 30:1, (d) 10:1, (e) 2:1 and (f) 1:1.

Fig. 3 shows the UV-vis spectra of the t-Te/Se ANRs fabricated with different molar ratios of TeO_2 to H_2SeO_3 ((a) 200:1, (b) 100:1, (c) 30:1, (d) 10:1, (e) 2:1 and (f) 1:1). The spectra show red shift with the Te proportion rising and the Se proportion dropping until the x(Te:Se) value of 30:1. There was little shift in the spectra between the ratios of 30:1 and 10:1. When the x(Te:Se) values decreased to 2:1 and to 1:1, blue shifts occurred. These significant spectral shifts might be assigned to the variation in the length of the t-Te/Se ANRs from 180 nm to 70 nm (red shifts), and then to 130 nm (blue shifts), which longer of the t-Te/Se ANRs led lower value of the wavelength.

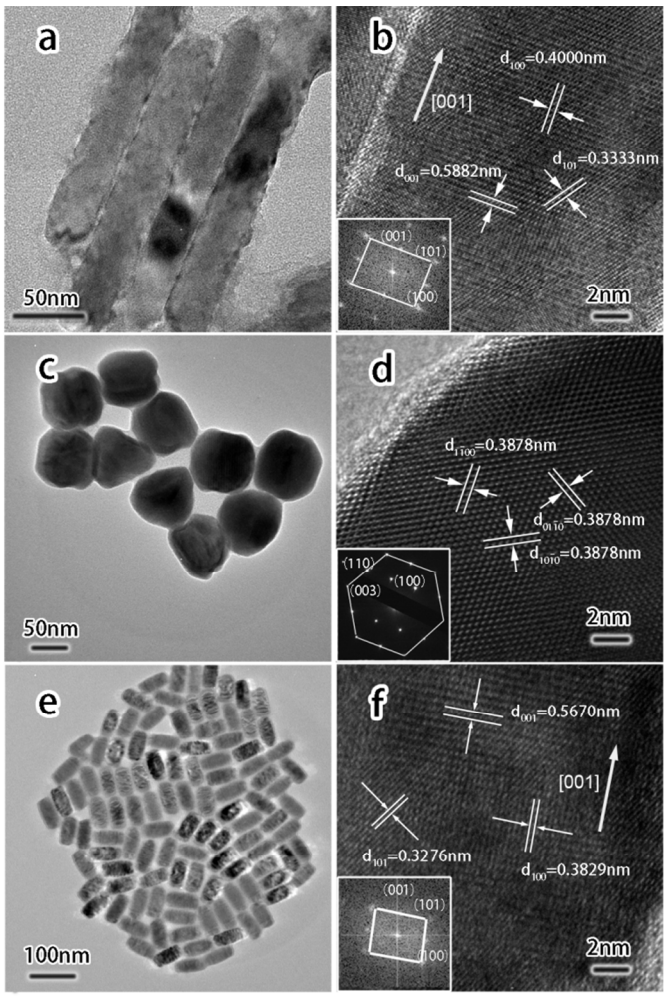

Fig. 4 t-Te/Se ANRs with x(Te:Se) = (a) 200:1, (c) 15:1 and (e) 1:1. (b), (d) and (f) are the HR-TEM images of t-Te/Se ANRs in (a), (c) and (e). The insets in (b), (f) indicate the Fast Fourier Transformation (FFT) and (d) is the electro-diffraction diagram.

The microstructures of the t-Te/Se ANRs were further analyzed by HR-TEM measurement (Fig. 4). Fig. 4a, c and e are when x(Te:Se) = 200:1, 15:1 and 1:1, respectively. The lattice fringes of Fig. 4b were 0.5882 nm, 0.4000 nm and 0.3333 nm which were corresponding to (001), (100) and (101) planes of t-Te/Se ANRs. (The lattice fringe spacings for t-Te and t-Se are listed as follows: Te_{001} =0.5926 nm, Te_{100} =0.3856 nm and Te_{101} =0.3233 nm (JCPDF NO: 36-1452), Se_{001} =0.4950 nm, Se_{100} =0.3780 nm and Se_{101} =0.3005 nm (JCPDF NO: 06-0362)). Fig. 4b shows that the t-Te/Se ANRs grew along the [001] direction. The HRTEM image of Fig. 4d was taken perpendicularly to the (001) plane of a t-Te/Se ATNR, and all the lattice spacings were 0.3878 nm that could be indexed to $(10\bar{1}0)$, $(01\bar{1}0)$ and $(1\bar{1}00)$ planes of the t-Te/Se ATNR, indicating that the t-Te/Se ATNRs also grew along the [001] direction as well. The lattice distances of the (110) and (003) planes calculated from the electro-diffraction diagram were 0.2260nm and 0.1934nm. The lattice fringe spacings in Fig. 4f were 0.5690 nm, 0.3829 nm and 0.3276nm respectively, corresponding to (001), (100) and (101) planes. Therefore, the nanorods with x(Te:Se) =1:1 tended to grow along the [001] direction as illustrated in Fig. 4f. The insets of Fig. 4b and f were Fast Fourier Transformation

(FFT) and the inset in the Fig. 4d was electron diffraction pattern.

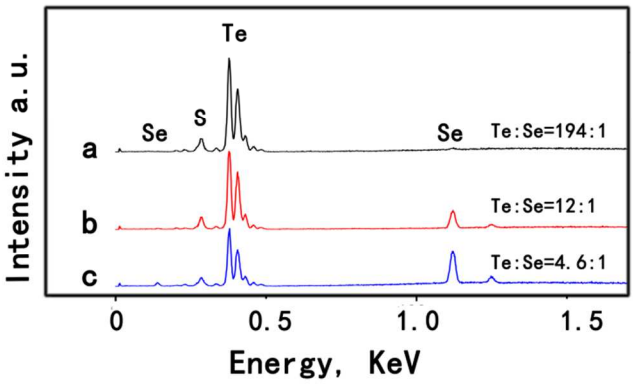

Fig. 5 EDAX spectra (a)-(c) that reveal the actual atom ratios of Te to Se in the t-Te/Se ANRs corresponding to Fig. 4(a), (c) and (e), which x(Te:Se) are 200:1, 15:1 and 1:1 respectively.

The real compositions of the t-Te/Se ANRs were clarified by EDAS (Fig. 5a, b and c). The initial x(Te:Se) in the precursors were (a) 200:1, (b) 15:1 and (c) 1:1 which were corresponding to Fig. 4a, c and e. The peaks of Se increased obviously with the x(Te:Se) decreasing, and the real values of Te:Se for the three groups of t-Te/Se ANRs were (a)194:1, (b) 12:1 and (c) 4.6:1. The 'S' peaks in the spectra were the sulphur element in SDS ($C_{12}H_{25}SO_4Na$) adhered to the t-Te/Se ANRs. The actual Se content in the nanorods was identical to that when x(Te:Se)=200:1 and 15:1, but it obviously increased when x(Te:Se)=1:1. This dramatic increase of Se content might be a result of the weaker crystal nature of Se than Te, so the nanorods tended to have more Te to ensure the high crystallinity of the t-Te/Se ANRs.[31]

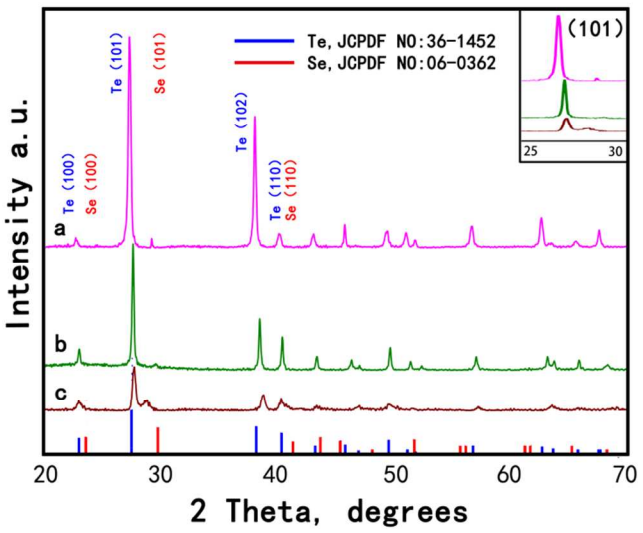

Fig. 6 XRD patterns of the t-Te/Se ANRs with three different values of x(Te:Se): (a) 200:1, (b) 15:1 and (c) 1:1. The peaks indicate that the t-Te/Se ANRs were single crystalline and belong to trigonal phase. The inset magnifies the (101) peaks of the three t-Te/Se ANRs.

The lattice constants of the t-Te/Se ANRs were analyzed by XRD (Fig. 6a, b and c). Alterations in the x(Te:Se) also led to ultimate changes in lattice constants of the t-Te/Se ANRs.

Fig. 6a, b and c show the XRD patterns of the nanorods corresponding to those in Fig. 4a, c and e, which the x(Te:Se) =200:1, 15:1 and 1:1, respectively. Those patterns were similar to those of pure Te (Blue line, JCPDF NO:36-1452) and Se (Red line, JCPDF NO:06-0362), indicating that the nanorods were well crystallized trigonal crystals. The peaks of (101) were also between the (101) peaks of pure t-Te and t-Se. The lattice constants were calculated and the results were between the pure t-Te (a =0.4458 nm, c =0.5927 nm) and the pure Se (a =0.4366 nm, c =0.4954 nm), which were (a) a =0.4516 nm, c =0.5895nm, (b) a =0.4454 nm, c =0.5874 nm, (c) a =0.4466 nm, c =0.5773 nm. With a higher percentage of Se, the 2-theta degrees of (101) peaks were getting closer to those of pure t-Se. In addition, the t-Te/Se ANRs fabricated with a lower proportion of Te and a higher proportion of Se in the ratio of Te to Se showed weaker intensity of XRD peaks, which can be seen obviously from the (101) peaks of Fig. 6a, b and c (Fig. 6 inset). That is probably because the intensity of XRD peaks of pure t-Se is weaker than that of pure t-Te.

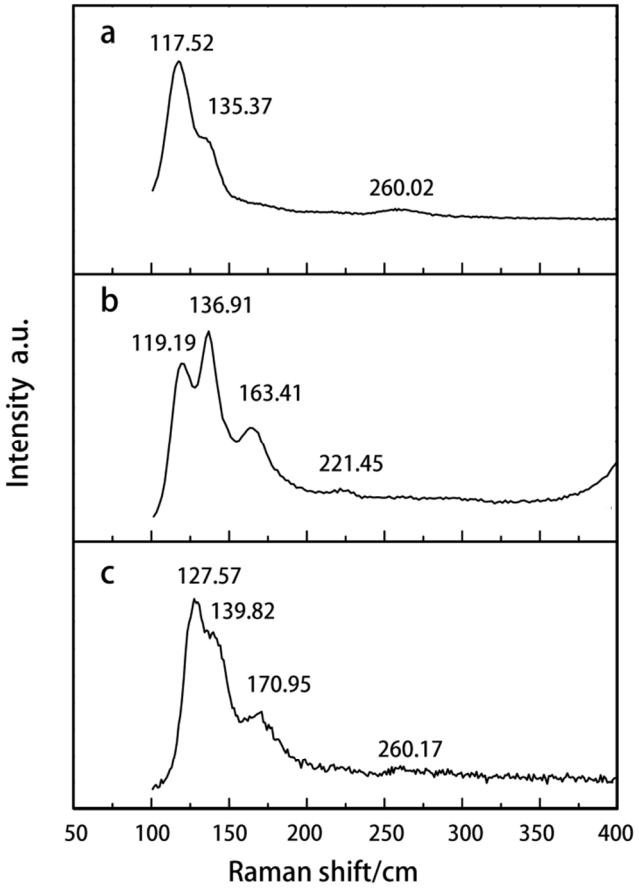

Fig. 7 Raman scattering specta of the t-Te/Se ANRs. The x(Te:Se) of the t-Te/Se ANRs are (a) 200:1, (b)15:1 and (c) 1:1.

The Raman spectra of t-Te/Se ANRs had been rarely studied. The x(Te:Se) of Fig. 7a, b and c were 200:1, 15:1 and 1:1 respectively. The peaks of the Fig. 7a were 117.52, 135.37 and

260.02 cm^{-1}. And the peaks of Fig. 7b were t-Te/Se ANRs were 119.19, 136.91, 163.41 and 221.45 cm^{-1}. The peaks of Fig. 7c were 127.57, 139.82, 170.95 and 260.17 cm^{-1}. These results were similar to the pure t-Te but shifted to high frequency.[36-38] This may be attributed to the Se added into the nanorods because pure t-Se had higher frequency Raman spectra. [39]And also different crystallinity between the materials can also lead to these results as well.[38]

Growth mechanism of t-Te/Se ANRs

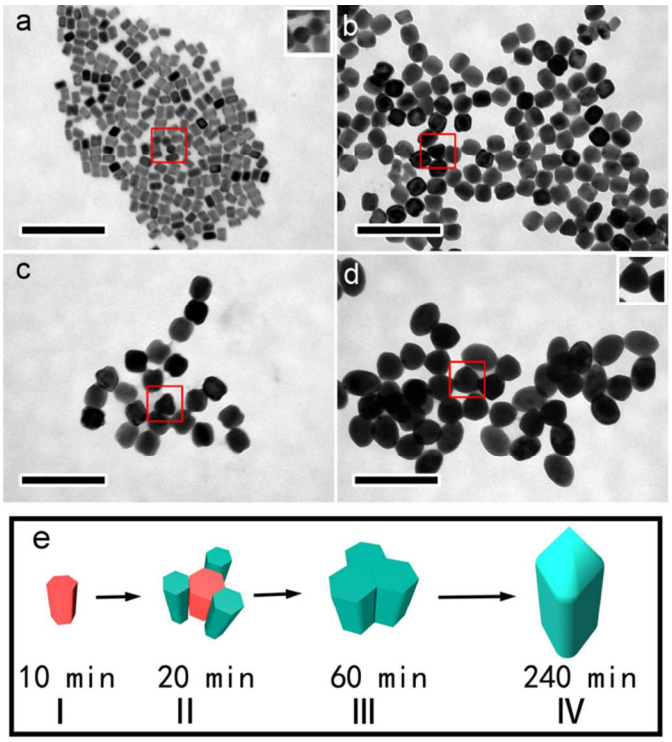

Fig. 8 TEM images showing the morphologies of the t-Te/Se ATNRs with x(Te:Se)=10:1 at time periods of (a)10 min, (b)20 min, (c) 60 min and (d) 240 min. Red frames circle the cross section of the nanorods. Insets in (a) and (d) are the cross section of the t-Te/Se ATNRs (a) and (d). (e) is the schematic of the t-Te/Se ATNRs evolution process. All of the scale bars in the pictures represent 200 nm.

The self-seeding nucleation and growth process were studied and the morphology transformation process was illustrated by TEM images. Fig. 8 shows the TEM images about the morphology evolution of t-Te/Se ATNRs with x(Te:Se)=10:1 at time periods of (a) 10 min, (b) 20 min, (c) 60 min and (d)240 min as well as the schematic of the four-step shape transformation (Fig. 8e). The growth mechanism of the t-Te/Se ATNRs followed that of tri-tips t-Te.[12] The t-Te/Se ATNRs grew first as small hexagonal prisms (Fig. 8a, a inset and e (Ⅰ)) within the period of 10 min, and then the Te and Se atoms selectively deposited at 3 surfaces of the initial hexagonal prism to form 3 new hexagonal prisms (Fig. 8b and e (Ⅱ)) within the period of 20 min. With further reduction and growth at 60 min, the 3 new hexagonal prisms became bigger and their central gap was filled up (Fig. 8c and e (Ⅲ)). Finally, the edges of the ATNRs became vaguer and the nanoparticles were in the shape of ellipsoid at 240 min (Fig. 8d and e (Ⅳ)).The inset in Fig. 7d is the cross section of the t-Te/Se ATNRs supporting this mechanism.

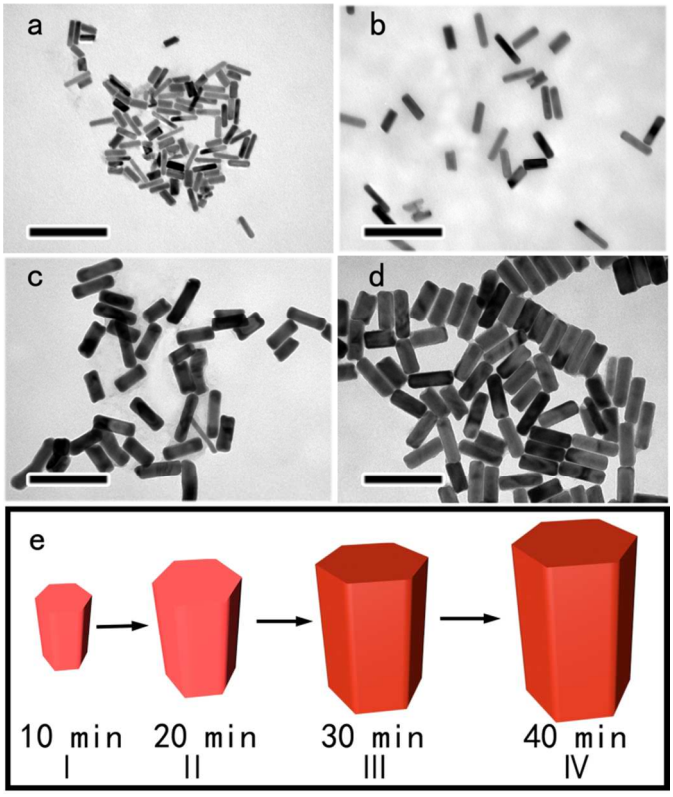

Fig. 9 TEM images of t-Te/Se ASNRs growth with x(Te:Se) =125:1 at time periods of (a) 10 min, (b)20 min, (c) 30 min and (d) 40 min. The SNRs just grew bigger as the reaction proceeded. (e) is the schematic of the t-Te/Se ASNRs evolution.

Fig. 9 shows TEM images of t-Te/Se ASNRs growth with x(Te:Se)=125:1 at time periods of (a) 10 min, (b)20 min, (c) 30 min and (d)40 min, within which the SNRs grew from 70±10 nm (Fig. 9a) to 140±15 nm(Fig. 9d) in length, and from 10±3nm to 40±5nm in diameter, indicating that the SNRs just became bigger as the redox reaction proceeded. The transformation process was similar to the growing process of the pure t-Te.[21]

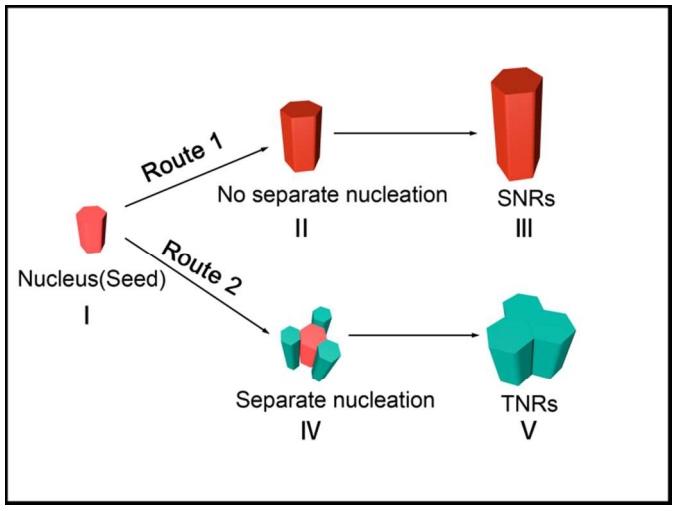

Fig. 10 Mechanism model for the two possible growth paths. Route 1 shows that the t-Te/Se ANRs grow directly from the initial hexagonal nuclear prisms (seeds) (Ⅰ) into t-Te/Se ASNRs (Ⅲ) without separate nucleation. Route 2 indicates that a separate nucleation leads to the transformation of the seeds into t-Te/Se ATNRs (Ⅳ). (Ⅱ) and (Ⅳ) grow bigger into (Ⅲ) and (Ⅴ), respectively, as the reaction proceeds.

Fig. 10 summarizes the two paths for the growth of t-Te/Se ANRs. Route 1 shows the general process about t-Te/Se ASNRs which Te and Se atoms initially to form hexagonal nucleus (seeds) (Fig. 10Ⅰ), and the Te/Se alloys only grew longer and wider (Fig. 10Ⅱ and Ⅲ) as the reaction progressed. Route 2 demonstrates the growing process for t-Te/Se ATNRs. The difference in Route 2 is that there is a separation nucleation process (Fig. 10Ⅳ) after the initial seed process, Te and Se atoms selectively deposited along the edge of the seed and leading the shape of t-Te/Se ANRs as TNRs. As the reaction continued, Fig. 10Ⅱ and Ⅳ grew bigger into Fig. 10 Ⅲ and Ⅴ, respectively. The TNRs phenomenon has been reported for pure Te NWs in water and ethylene glycol mixture in high temperature or pressure, but little information is available about the TNRs of Te/Se alloys.[12, 40, 41]

The evolution mechanism was as follows: The Te and Se atoms were formed as Te-Se boned helical chains[11], these chains disorganized aggregated as amorphous Te/Se (a-Te/Se) at the initial moment, then the a-Te/Se (disorganized chains) transformed to trigonal Te/Se (organized chains) because of Reyleigh instability[13]. The EDS spectra of Fig. 7a and Fig. 8a (Fig. S2, ESI†) showed the real Te:Se values were 13:1 and 124:1 respectively, which means the seeds were Te/Se alloys.

This phenomenon may be attributed to the difference in both chemical kinetics and crystal kinetics. The H_2SeO_3 can be more easily reduced than the TeO_2, suggesting that H_2SeO_3 [31] is higher than TeO_2 in reduction potential.[26] Additionally, Te belongs to metalloid with a more obvious crystalline nature than Se which is non-metallic with the amorphous nature.[31] When Te and Se began to form homogenous nanorods, their morphologies would be influenced by the competition between the crystalline tendency of Te to grow into trigonal Te and the amorphous tendency of Se to grow into amorphous Se, suggesting that the nanostructure of t-Te/Se ANRs was sensitive to the original value of x(Te:Se). Therefore, when x(Te:Se)=200:1 and 100:1, the trigonal Te nature dominated the morphology, which was similar to pure t-Te.[11, 21] When x(Te:Se) = 2:1 and 1:1, the trigonal Se nature played the defining role in morphology, which was identical to pure t-Se.[13] Only when the x(Te:Se) ranged from 30:1 to 10:1 could the t-Te/Se ANRs grow into TNRs under the mutual effects of Te and Se chemical and crystal properties.

Conclusions

We have developed a practical protocol for controllable generation of t-Te/Se ANRs with various morphologies by varying the reaction conditions, which tuned from long and thin SNRs to TNRs and back to shuttle-like SNRs. The lattice constants and compositions of nanorods also varied with changes in the initial molar ratio of TeO_2 to H_2SeO_3. All the t-Te/Se ANRs possess distinct morphology prosperities in terms of uniformity and monodispersity. These high-quality nanomaterials remain stable in water for months.

As the compositions, morphologies and lattice constants can be well designed by tuning parameters for the reaction, the novel high quality nanostructures may have potential applications in thermoelectricity and photoconductivity and can also be used as a sacrificial template for synthesis of complex noble metal nanostructures like Au nanoframes.[1, 42, 43]

Acknowledgements

We gratefully acknowledge the financial support from National Natural Science Foundation of China (21375043, 21175051).

Notes and references

[a] State Key Laboratory of Agricultural Microbiology, College of Science. Huazhong Agricultural University, Wuhan 430070, P.R. China.
E-mail: hyhan@mail.hzau.edu.cn.

† Electronic Supplementary Information (ESI) available: TEM image of reaction conditions for amorphous Te/Se alloys were x(Te:Se)=1:10 and growth time of 10 min. See DOI:10.1039/b000000x/

1. K. Cai, Z. Lv, K. Chen, L. Huang, J. Wang, F. Shao, Y. Wang and H. Han, *Chem. Comm.*, 2013, **49**, 6024-6026.
2. G. Zhang, H. Fang, H. Yang, L. A. Jauregui, Y. P. Chen and Y. Wu, *Nano Lett.*, 2012, **12**, 3627-3633.
3. H. H. Li, P. Zhang, C. L. Liang, J. Yang, M. Zhou, X. H. Lu and G. A. Hope, *Cryst. Res. Technol.*, 2012, **47**, 1069-1074.
4. W. S. Wang, J. Goebl, L. He, S. Aloni, Y. X. Hu, L. Zhen and Y. D. Yin, *J. Am. Chem. Soc.*, 2010, **132**, 17316-17324.
5. F. K. Butt, M. Mirza, C. Cao, F. Idrees, M. Tahir, M. Safdar, Z. Ali, M. Tanveer and I. Aslam, *CrystEngComm*, 2014, **16**, 3470-3473.
6. N. P. Dasgupta, J. Sun, C. Liu, S. Brittman, S. C. Andrews, J. Lim, H. Gao, R. Yan and P. Yang, *Adv. Mater.*, 2014, **26**, 2137-2184.
7. Z. Wang, L. Wang, J. Huang, H. Wang, L. Pan and X. Wei, *J. Mater. Chem.*, 2010, **20**, 2457.
8. H. Xu, G. Chen, R. Jin, D. Chen, Y. Wang, J. Pei, Y. Zhang, C. Yan and Z. Qiu, *CrystEngComm*, 2014, **16**, 3965-3970.
9. L. D. Zhao, S. H. Lo, Y. Zhang, H. Sun, G. Tan, C. Uher, C. Wolverton, V. P. Dravid and M. G. Kanatzidis, *Nature*, 2014, **508**, 373-377.
10. B. Sadtler, S. P. Burgos, N. A. Batara, J. A. Beardslee, H. A. Atwater and N. S. Lewis, *Proc. Natl. Acad. Sci. U S A*, 2013, **110**, 19707-19712.
11. B. Mayers, B. Gates, Y. Yin and Y. Xia, *Adv. Mater.*, 2001, **13**, 1380-1384.
12. B. Mayers and Y. Xia, *J. Mater. Chem.*, 2002, **12**, 1875-1881.
13. B. Gates, B. Mayers, B. Cattle and Y. N. Xia, *Adv. Funct. Mater.*, 2002, **12**, 219-227.
14. Z.-H. Lin, P. Roy, Z.-Y. Shih, C.-M. Ou and H.-T. Chang, *ChemPlusChem*, 2013, **78**, 302-309.
15. K. Sridharan, M. S. Ollakkan, R. Philip and T. J. Park, *Carbon*, 2013, **63**, 263-273.
16. Z. Li, S. Zheng, Y. Zhang, R. Teng, T. Huang, C. Chen and G. Lu, *J. Mater. Chem. A*, 2013, **1**, 15046.
17. Q. Wang, M. Safdar, X. Zhan and J. He, *CrystEngComm*, 2013, **15**, 8475-8482.
18. J. Pei, G. Chen, D. Jia, R. Jin, J. Sun and Y. Yu, *CrystEngComm*, 2013, **15**, 241-244.
19. C. Chen, Y. Kang, Z. Huo, Z. Zhu, W. Huang, H. L. Xin, J. D. Snyder, D. Li, J. A. Herron, M. Mavrikakis, M. Chi, K. L. More,

Y. Li, N. M. Markovic, G. A. Somorjai, P. Yang and V. R. Stamenkovic, *Science*, 2014, **343**, 1339-1343.
20. H. Zhu, J. Luo, H. Zhang, J. Liang, G. Rao, J. Li, G. Liu and Z. Du, *CrystEngComm*, 2012, **14**, 251-255.
21. Z.-H. Lin, Z. Yang and H.-T. Chang, *Cryst. Growth Des.*, 2008, **8**, 351-357.
22. C. J. Hawley, B. R. Beatty, G. Chen and J. E. Spanier, *Cryst. Growth Des.*, 2012, **12**, 2789-2793.
23. B. Zhang, W. Hou, X. Ye, S. Fu and Y. Xie, *Adv. Funct. Mater.*, 2007, **17**, 486-492.
24. H. S. Qian, S. H. Yu, J. Y. Gong, L. B. Luo and L. F. Fei, *Langmuir : the ACS journal of surfaces and colloids*, 2006, **22**, 3830-3835.
25. J. Zhang, S.-Y. Zhang and H.-Y. Chen, *Chem. Lett.*, 2004, **33**, 1054-1055.
26. U. Y. Jeong and Y. N. Xia, *Adv. Mater.*, 2005, **17**, 102-106.
27. X. M. Li, Y. Li, S. Q. Li, W. W. Zhou, H. B. Chu, W. Chen, I. L. Li and Z. K. Tang, *Cryst. Growth Des*, 2005, **5**, 911-916.
28. J.-W. Liu, J.-H. Zhu, C.-L. Zhang, H.-W. Liang and S.-H. Yu, *J. Am. Chem. Soc.*, 2010, **132**, 8945-8952.
29. Q. Wang, M. Safdar, Z. Wang and J. He, *Adv. Mater.*, 2013, **25**, 3915-3921.
30. R. M. Ireland, L. Zhang, P. Gopalan and H. E. Katz, *Adv. Mater.*, 2013, **25**, 4358-4364.
31. G. Kaur and M. S. Bakshi, *J. Phys. Chem. C*, 2010, **114**, 143-154.
32. D.-h. Qin, H. Tao and Y. Cao, *Chinese J. Chem. Phy.*, 2007, **20**, 670-674.
33. B. Zhou and J.-J. Zhu, *Nanotechnology*, 2006, **17**, 1763-1769.
34. T. P. Vinod, M. Park, S. H. Kim and J. Kim, *Langmuir*, 2010, **26**, 9195-9197.
35. H. Tao, X. Shan, D. Yu, H. Liu, D. Qin and Y. Cao, *Nanoscale Res. Lett.*, 2009, **4**, 963-970.
36. S. Wang, K. Zhang, H. Zhou, W. Guan, D. Ma, J. Lin, L. Zhang, S. Huang and J. Wang, *CrystEngcomm*, 2010, **12**, 3852-3857.
37. J.-W. Liu, F. Chen, M. Zhang, H. Qi, C.-L. Zhang and S.-H. Yu, *Langmuir*, 2010, **26**, 11372-11377.
38. J. M. Song, Y. Z. Lin, Y. J. Zhan, Y. C. Tian, G. Liu and S. H. Yu, *Cryst. Growth Des.*, 2008, **8**, 1902-1908.
39. L. Liu, Q. Peng and Y. Li, *Nano Res.*, 2008, **1**, 403-411.
40. S. Wang, W. Guan, D. Ma, X. Chen, L. Wan, S. Huang and J. Wang, *CrystEngComm*, 2010, **12**, 166-171.
41. L. Yang, Z.-G. Chen, G. Han, L. Cheng, H. Xu and J. Zou, *Cryst. Growth Des.*, 2013, **13**, 4796-4802.
42. M. McEachran, D. Keogh, B. Pietrobon, N. Cathcart, I. Gourevich, N. Coombs and V. Kitaev, *J. Am. Chem. Soc.*, 2011, **133**, 8066-8069.
43. N. R. Sieb, N. C. Wu, E. Majidi, R. Kukreja, N. R. Branda and B. D. Gates, *Acs Nano*, 2009, **3**, 1365-1372.

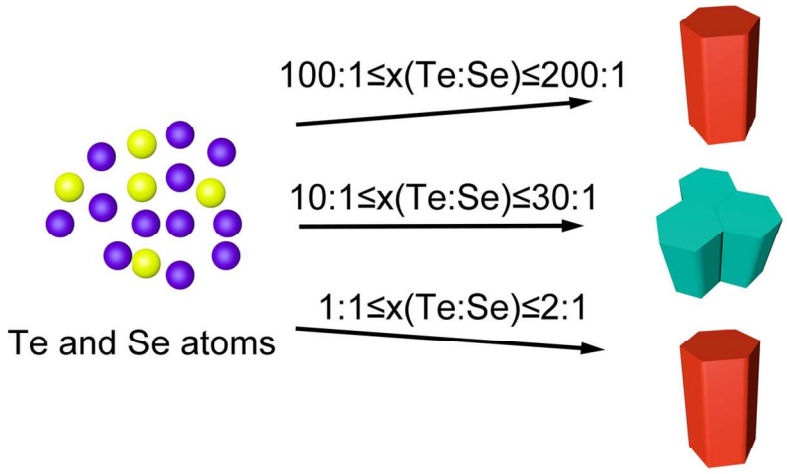

The nanostructures of Te/Se alloy nanorods were single nanorods when the molar ratio of TeO2 to H2SeO3 (x(Te:Se)) ranging from 200:1 to 100:1 or 2:1 to 1:1, and were tri-fold nanorods when x(Te:Se) ranging from 30:1 to 10:1.
64x41mm (600 x 600 DPI)